CARBON letters

Original Articles
Carbon Letters Vol. 27, 98-107 (2018)

A novel free-standing anode of CuO nanorods in carbon nanotube webs for flexible lithium ion batteries

Sehyun Lee[1,*], Hyeonjun Song[2,*], Jun Yeon Hwang[3], Seung Min Kim[3] and Youngjin Jeong[1,2,♠]

[1]Department of Organic Materials and Fiber Engineering, Soongsil University, Seoul 06978, Korea
[2]Department of Information Communication, Materials, and Chemistry Convergence Technology, Soongsil University, Seoul 06978, Korea
[3]Carbon Convergence Materials Research Center, Institute of Advanced Composite Materials, Korea Institute of Science and Technology (KIST), Wanju 55324, Korea

Article Info
Received 17 August 2017
Accepted 20 October 2017

♠Corresponding Author
E-mail: yjeong@ssu.ac.kr
Tel: +82-
*The authors have contributed equally in discussions of the work, performing the experiments, and writing the paper.

Open Access
DOI: http://dx.doi.org/10.5714/CL.2018.27.098

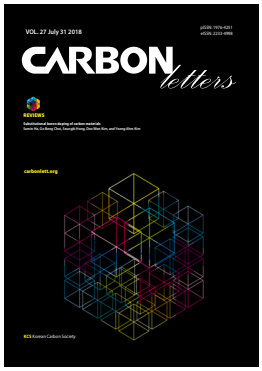

http://carbonlett.org

pISSN: 1976-4251
eISSN: 2233-4998

Abstract

Free-standing electrodes of CuO nanorods in carbon nanotubes (CNTs) are developed by synthesizing porous CuO nanorods throughout CNT webs. The electrochemical performance of the free-standing electrodes is evaluated for their use in flexible lithium ion batteries (LIBs). The electrodes comprising CuO@CNT nanocomposites (NCs) were characterized by charge-discharge testing, cyclic voltammetry, and impedance measurement. These structures are capable of accommodating a high number of lithium ions as well as increasing stability; thus, an increase of capacity in long-term cycling and a good rate capability is achieved. We demonstrate a simple process of fabricating free-standing electrodes of CuO@CNT NCs that can be utilized in flexible LIBs with high performance in terms of capacity and cycling stability.

Key words: copper oxide, carbon nanotube, free-standing electrode, lithium ion battery, flexible battery

1. Introduction

The electronics industry has developed very light and thin electronics that have contributed to the advent of small-sized, potentially flexible lithium ion batteries (LIBs) [1]. A number of studies to develop flexible LIBs have been conducted in response to the market growth of flexible electronics [2-16]. Existing batteries have shortcomings when applied to the flexible electronics because conventional electrode materials are not mechanically flexible [2]. In addition, the electrodes prepared through a typical slurry method are not suitable for use in flexible LIBs since the active materials have weak adhesion to the metal current collectors [2,10,17]. To overcome the above problems, many studies have employed free-standing electrodes that are fabricated without using a polymer binder [3,4]. Some have focused on methods of fabricating flexible electrodes by incorporating active materials into a flexible matrix, such as carbon nanotube (CNT) powders [3,4,8,9] and graphene sheets [6,7]. However, the fabricated flexible matrix did not maintain its structure under external influences such as bending; it also suffered from low mechanical strength due to a weak cohesive bonding [2,3].

Recently, the metal oxide of CuO has drawn attention because of its low-cost, chemical stability, high theoretical capacity (674 mAh g^{-1}) and availability on the Earth [17-20]. However, a pure CuO electrode in LIBs has experienced a morphological breakage caused by the volume changes during cycling which leads to poor cycleability and low capacity. Our previous study utilized CNT webs as a free-standing electrode. The study showed the CNTs' promising use in flexible LIBs; however, CNTs exhibit high irreversible capacity loss at the first cycle because of the formation of a solid electrolyte interface (SEI) throughout the large surface area of the active CNT webs [21]. This study illustrates that CNT web electrodes

have the advantages of high flexibility and good functionality as current collectors. However, they are plagued with unwanted SEI formation, which causes very low capacity.

In this work, CNT webs were employed to study their roles as a current collector as well as a flexible scaffold for CuO nanorods (NRs). In order to overcome the limitation of pure CuO electrodes and to utilize the advantages of the CNT webs, a free-standing electrode (forest-like CuO@CNT NCs) was fabricated by growing the CuO NRs on the bundle surface of the CNT webs. The CuO nanoparticles (NPs) in the CuO@CNT NCs were generated by disintegrating the CuO NRs during repeated cycling because the CNT web, which has a network structure consisting of long CNT bundles, provides effective long electron pathways for CuO. This study evaluates the performance of the CuO@CNT NCs as an anode material for LIBs.

2. Experimental

2.1. CNT synthesis and negatively charged CNT webs

For the synthesis of CNT webs, acetone (99.7%) was purchased from Samchun Chemical (Korea). Ferrocene (≥98%), thiophene (≥99%), and polysorbate 20 were purchased from Sigma Aldrich (USA). To prepare the CuO precursor solution, copper nitrate trihydrate ($Cu(NO_3)_2$•$3H_2O$, 98%), ammonium hydroxide (NH_4OH, 28%) and sodium dodecylsulfate (SDS; $CH_3(CH_2)_{11}OSO_3Na$) were purchased from Sigma Aldrich. All reagents were analytical grade and used without further purification. Subsequently, acetone 98.0 wt%, ferrocene 0.2 wt%, and thiophene 0.8 wt% were used to synthesize the negatively charged CNT webs. The solution was injected at a rate of 10 mL h^{-1} with hydrogen gas flowing at a rate of 1100 sccm into a vertical reactor heated to 1200°C. The CNTs were continuously synthesized and wound up at 4 m min^{-1} using a winder system to form CNT webs. The synthesis and properties of the CNT webs were described in detail in our previous studies [22,23]. A 10 mg amount of SDS was added to DI water (100 mL) to dilute the SDS solution. With a ratio of SDS to CNT webs of 1/1 wt%, 10 mg of the CNT webs was dipped into the diluted SDS solution for 3 h. As shown in Fig. 1A, the negatively-charged CNT webs with sulfate were retrieved from the SDS solution with tweezers [17].

2.2. Fabrication of CuO@CNT NCs

To fabricate CuO NRs in the CNT webs, 10 mL of the ammonium hydroxide was diluted with distilled water (DI; 10 mL) to reach a pH solution of 12.6; subsequently, 0.5 M (1.205 g) of copper nitrate trihydrate ($Cu(NO)_3)_2 \cdot 3H_2O$) was dissolved in the diluted solution at room temperature. After sufficient dissolution for 30 min, the temperature of the solution was raised and maintained at 60°C until $Cu(OH)_2$ precipitates were observed in the solution. Using a 0.6 μm filter paper, these precipitates were removed by filtering the solution. Then, the solution was adjusted to pH 9.0 by adding DI water and stirring vigorously for 10 min. The stirred solution became opaque in a couple of seconds. The regenerated $Cu(OH)_2$ precipitates in the solution were filtered again using the same filter paper. Afterwards, the $Cu(NO_3)_2$ saturated solution was obtained as shown in Fig. 1B.

CuO@CNT NCs were synthesized by adding the negatively charged CNT webs to the saturated solution (Fig. 1C). In the mixed solution, the $Cu(OH)_2$ was nucleated on the surface of the CNT fibers that were intermingled in a three-dimensional structure of CNT webs. This led to the growth of CuO by the electrostatic-driven attraction between the positive $Cu(OH)_2$ and the negative sulfate ions on the CNT webs [24]. While the

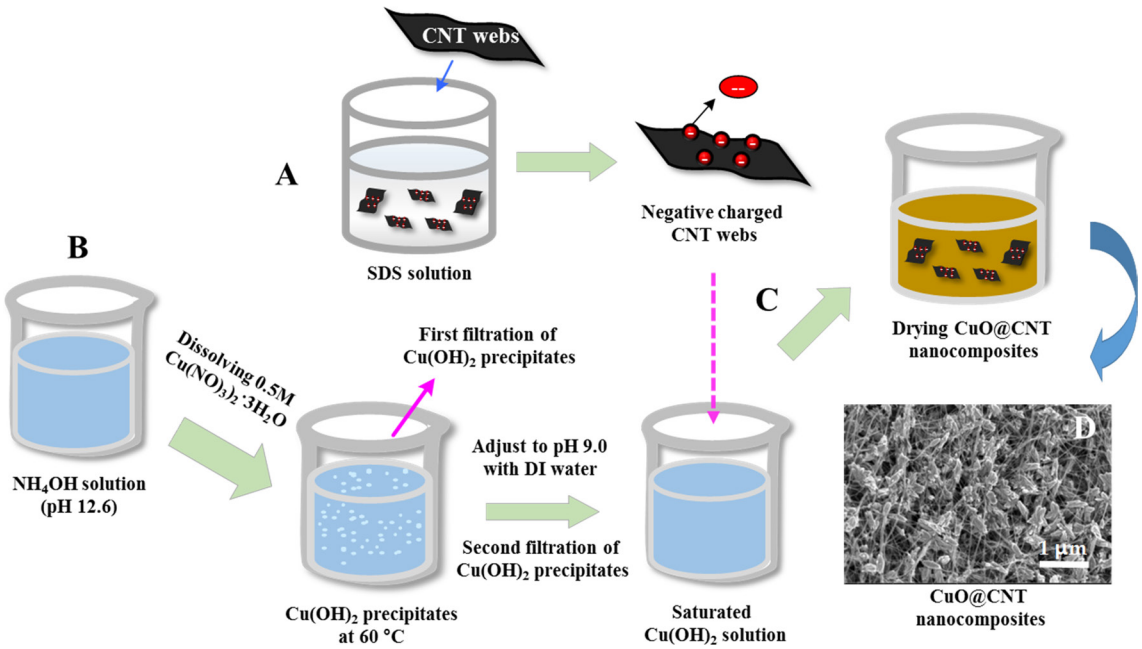

Fig. 1. Schematic illustration showing the synthesis procedure of the forest-like CuO@CNT NCs.

mixed solution was maintained at 60°C for 1 h, the $Cu(OH)_2$ was transformed into mesoporous CuO particles. At this time, the color of this solution changed from sky blue to dark brown. The final NCs were prepared for the free-standing electrode by drying them in a 120°C vacuum oven for 12 h (Fig. 1D). The actual mass of CuO NPs was measured by comparing the mass of CNT webs with one of the CuO@CNT NCs. The actual weight of CuO NPs in the electrode was around 1.5 mg cm^{-2}. Otherwise, the weight ratio of CuO NPs to CNT webs in the NCs was around 3 to 2.

2.3. Cell fabrication

The samples were assembled into a typical half-cell configuration using CR2032 coin cells (MTI Korea). These coin cells were assembled in an argon glove box (Korea Kiyon, Korea) using a Celgard 2325 separator and a lithium (Li) metal foil (450 μm thick). The free-standing CuO@CNT NCs were used as a working electrode and Li metal as a counter electrode. A mixture of 1.1M $LiPF_6$ in ethylene carbonate/diethylene carbonate (1:1 by volume, Wellcos, Korea) was used as an electrolyte for all the coin cells. Galvanostatic charge/discharge tests were performed at current rates of 0.5 C in the voltage range of 0.01-3.00 V with the use of charge/discharge cyclers (Shin Corp., Korea) at room temperature. Cyclic voltammograms (CVs) of the electrode were performed within a voltage window of 0 to 3.0 V versus Li/Li+ at a scan rate of 0.5 mV s^{-1} using PGSTAT 302N (Metrohm Autolab, the Netherlands). The assembled cells were aged for 10 h before measurement. The cells were analyzed via electrochemical impedance spectroscopy (PGSTAT 302N, Autolab) in a frequency range of 10 mHz to 0.1 MHz. The measurement of the assembled cells was performed after three cycles.

2.4. Characterization

To characterize the electrode structures, a Raman spectrometer (LabRAM HR UV-visible NIR, HORIBA, Japan) with an argon laser at a wavelength of 632.8 nm and X-ray diffraction (XRD; SmartLab, Ringaku, Japan) using Cu Kα radiation were used. The morphologies of the samples were analyzed by a field emission SEM (FEI, Verios 460 L). The cross section structures of the samples were investigated using FEI Helios NanoLab 650 focused ion beam. Transmission electron microscopy (TEM) images were taken using a FEI Tecnai G2 F20 electron microscope operating at 200 kV.

3. Results and Discussion

3.1. Characterization of CNT webs and CuO@CNT NCs

Two types of CuO materials were formed during their synthesis. One was the CuO NRs that were mainly formed on the surface of CNT fibers. The other was the CuO NPs that were dispersed throughout the CNT fibers. The TEM image of the CuO NRs shows the shape of the powdered particles, which were around 1 μm in length and a few hundred nanometers in width (inset of Fig. 2a). A representative HRTEM image for the CuO NRs displays an interplanar spacing of about 0.23 nm, which represents the spacing of the (111) plane of the CuO cubic structure (Fig. 2b) [17].

In particular, many pores in the CuO particles were formed during the synthesis and the average pore diameter was around 4 nm (noted by arrows in Fig. 2a). The CNT webs produced via direct spinning method were very flexible and consisted of several continuous fibers with diameters of around 20 nm. The CNT webs formed a 3-dimensional network structure with flexibility, high electrical conductivity (ca.10^5 S m^{-1}), good mechanical strength and high surface area [25]. As seen in Fig. 2d, the free-standing electrode made with the prepared CuO@CNT NCs illustrates the numerous CuO particles in the network structure of the CNT webs. Even with the numerous CuO NRs incorporated throughout the CNT webs, the CuO@CNT NCs exhibited good flexibility (Fig. 2e). This is also attributed to the network structure of the CNT webs by nature [21].

Since the CNT webs featured three-dimensional network structures, it was easy for the seed of the CuO NRs to penetrate into the network structure where the CuO NRs were formed (inset of Fig. 2d). Some of the CuO NPs were settled on the CNT fibers; that is, the CuO NPs were seen as tiny particles (around 5 nm) in the TEM image (Fig. 2c) [17]. Thus, it can be inferred that the CuO started nucleating on the surface of the CNT fiber. As shown in Fig. 2c, the fast Fourier transform pattern of the TEM image confirmed the CuO particles in the CNT structure. The lattice fringe spacing was about 0.245 nm, which was consistent with the (111) planes in monoclinic CuO and the 0.212 nm fringe spacing indicated in the (200) planes. In comparison, there was a clear distinction in Fig. 3 between a single fiber of a pristine CNTs and the CuO@CNT NCs.

Some studies have reported that mesoporous anode materials

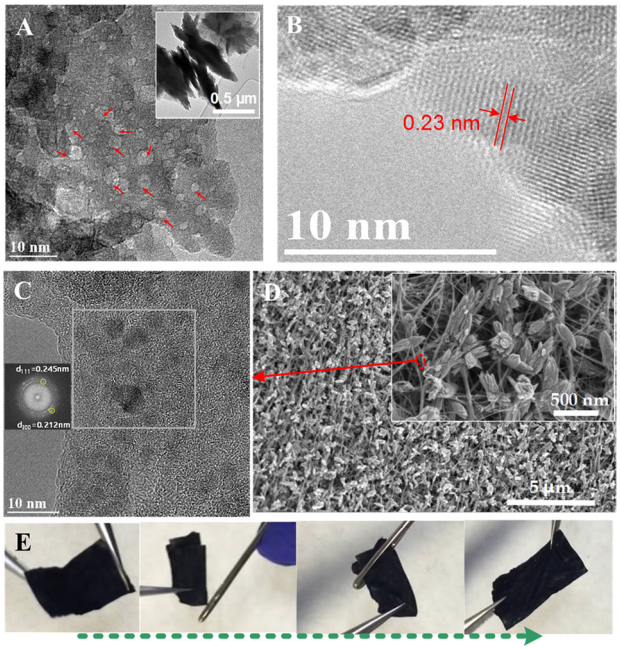

Fig. 2. TEM images of CuO NRs (a, b) and TEM image (c) of a single CuO@CNT fiber and SEM image (d) of CuO@CNT NCs and a series of photo images (e) illustrating the flexibility of CuO@CNT NCs.

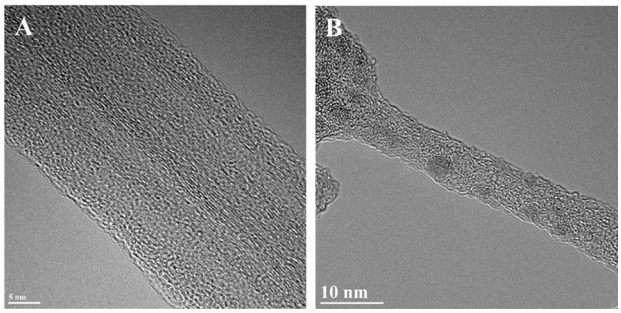

Fig. 3. Comparison of TEM image of pristine CNT fiber (a) with one of the CNT fibers in pristine CuO@CNT NCs (b).

could largely enhance capacity retention since the pore structures absorb the impact from and external stress induced by the volume changes during cycling [17]. However, we found that the large CuO NRs with a mesoporous structure broke into tiny CuO particles during cycling. This will be dealt with in the discussion of electrochemical reaction. Meanwhile, other researchers improved the cycling performance by covering the porous anode materials with carbon or graphene [26,27]. This suggests that the mesoporous structures by themselves could not prevent the pulverization issue during cycling.

The CNT webs before and after the CuO formation were characterized by Raman spectroscopy to analyze the changes in their crystalline qualities. In general, the intensity ratio of the G-band to the D-band (I_G/I_D) can be used to evaluate the degree of crystalline perfection [28,29]. The I_G/I_D ratio of the pristine CNT webs was 6.67, which was higher than the ratio (4) of the CuO@CNT NCs (Fig. 4a) [21,25].

As shown in Fig. 4b, the CuO materials were well-synthesized according to the observation of the XRD peaks [17,21,30]. Several well-defined diffraction peaks were observed at 32.5, 35.6, 38.7, 48.7, 53.5, 58.0, 66.2 and 68.1; these corresponded to the (110), (002), (111), (202), (020), (202), (022) and (220) planes of CuO, respectively. EDX elemental mapping was carried out to verify the spatial distribution of Cu, O, and C in the CuO@CNT NCs (Fig. 4c-f). The mapping images indicated that the carbon (C) element was evenly distributed. The copper (Cu) and oxygen (O) exhibited some sort of patterns by the shape of their formation. In particular, the "Cu" showed patterns similar to the "O" which indicated that the two elements were well-combined.

3.2. Electrochemical properties of CuO@CNT NCs electrodes

Fig. 5a shows the CVs of the electrode for the 1st, 2nd and 3rd cycles which characterize the electrochemical reactions. In the first cycle, there were three cathodic peaks at around 0.28, 0.96 and 1.75 V, suggesting that multi-step electrochemical reactions occurred [30-32]. That phenomenon was due to the reduction of CuO to Cu_2O as well as the partial formation of a reversible SEI layer ($2CuO+2Li^+ \rightarrow Cu_2O+Li_2O$) at a voltage higher than 0.96 V. At a lower voltage (>0.28 V), the additional formation of Cu_2O to Cu and Li_2O ($Cu_2O+2Li^+ \rightarrow 2Cu+Li_2O$) occurred. During the second and third cycles, the cathodic peaks shifted positively with a clear decrease in intensity. Meanwhile, three oxidation peaks were observed at 1.41, 2.45 and 2.70 V in the first anodic scan process, which were related to the formation of Cu_2O and CuO and the partial decomposition of an SEI layer [30,31]. From the second cycle, the CV profiles remain similar. We inferred that the reduction and oxidation reaction with the subsequent cycles were repeated with-

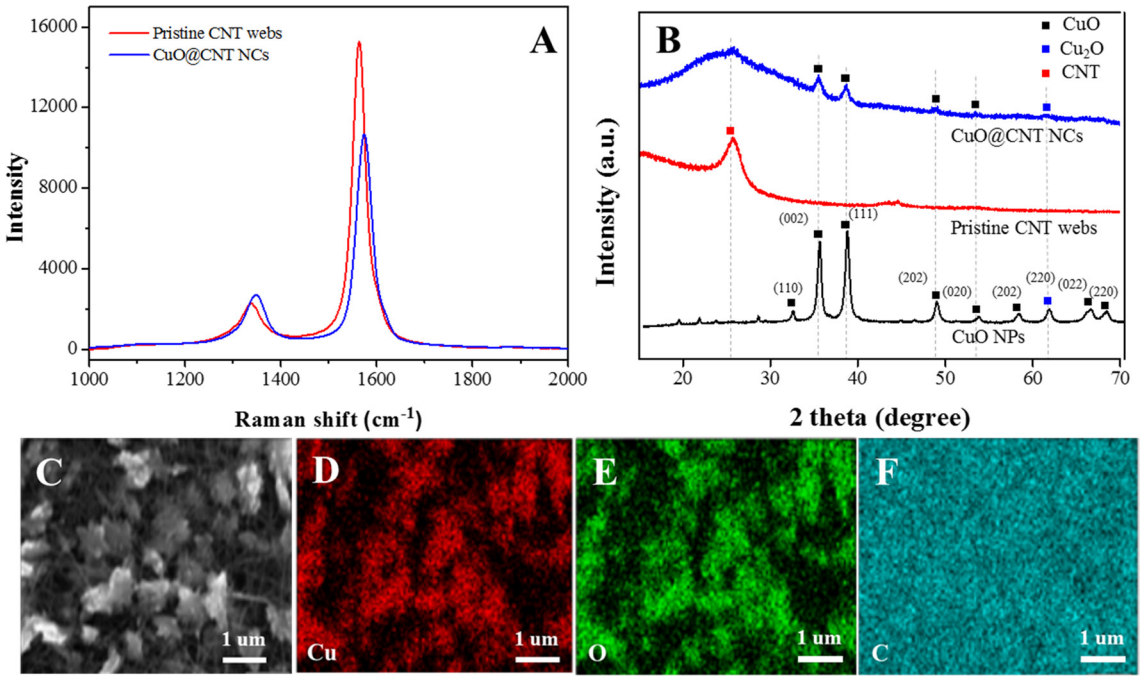

Fig. 4. Raman spectra and XRD profiles of the pristine CNT webs and the CuO@CNT NCs (a, b) and (d-f) elemental mapping images of the forest-like CuO@CNT NCs shown in (c). The XRD profile of (b) was obtained using bulk CuO NPs.

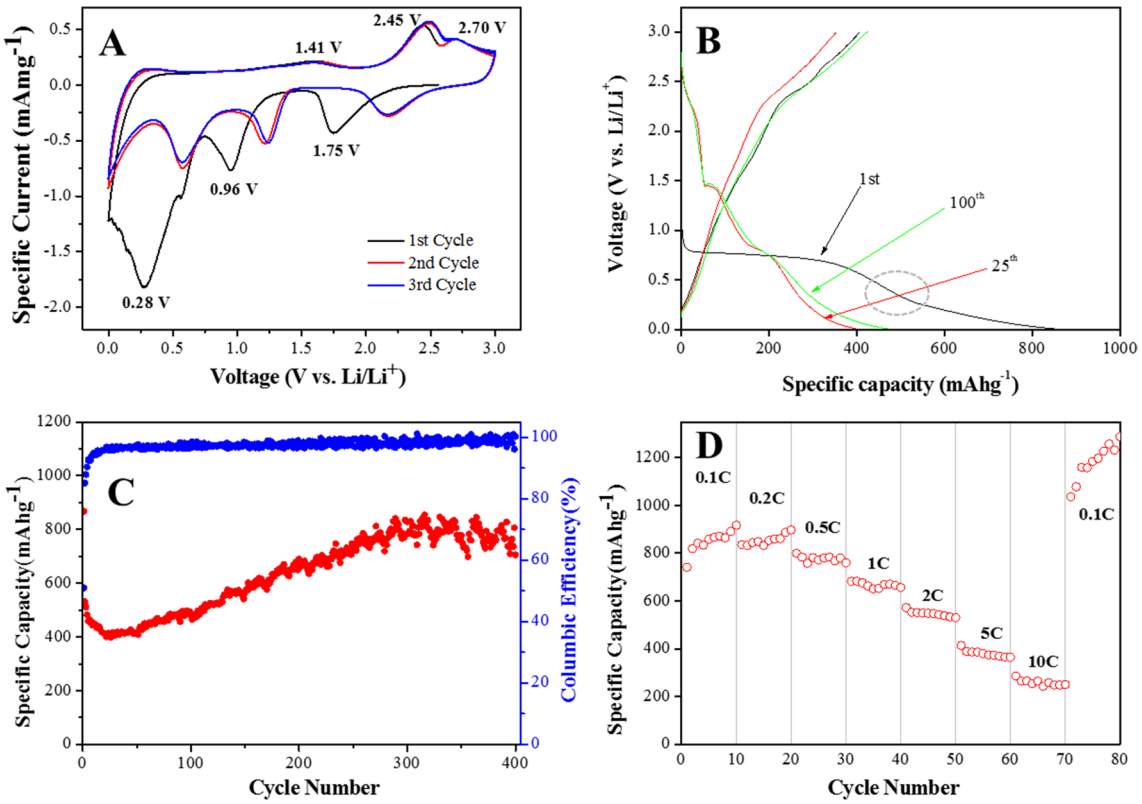

Fig. 5. Electrochemical performance of a forest-like CuO@CNT NC electrode: (a) representative cyclic voltammograms (CVs); (b) charge–discharge voltage profiles at a current density of 0.5 C; (c) cycling performance and Coulombic efficiency at current densities of 0.5 C; (d) rate capability at different current densities.

out a profile change. This resulted in a reversible electrochemical reaction in the CuO@CNT NCs electrode system. Furthermore, since the CNT web was grown on a metallic catalyst, the CNT web contained about 20% metallic catalyst impurities [33]. However, there were no peaks associated with side reactions shown in the CV curves, which means that the CNT web is a suitable material for a current collector of CuO.

The voltage profiles of galvanostatic charge-discharge at several cycles (1st, 25th and 100th) were plotted at a 0.5 C rate within the same potential range as shown in Fig. 5b. The first discharge curve for CuO@CNT NCs shows three steps at 0.1–0.4 V, 0.4–0.8 V, 0.8–0.9 V and over 0.9 V. Around 0.4 V, there was a slight inflection point (marked with a dotted circle), which had a large plateau at around 0.85 V, which was influenced by the large surface area of the CNTs but was noticeably different from the CNT curves [34].

The empty spaces in the network of the CuO@CNT NCs electrode resulted in the generation of non-active CuO particles that were at a distance from the CNT fibers. There were no electrical channels to collect the electrons generated by the electrochemical reaction between the CuO particles and Li ions since the free-standing electrode does not contain electric conducting powders in the electrode. Due to the presence of non-active materials, the capacities from the 1st to around the 25th cycle kept decreasing until the CuO particles in the electrode were stabilized. After the 25 cycles, the capacity of the free-standing CuO@CNT NC electrode gradually increased during the next 300 cycles and reached around 860 mAh g^{-1}; that value was about a 200% increase over the initial capacity (400 mAh g^{-1}) in Fig. 5c. The difference may be indirectly related to the cycling performance between the CuO@CNT NCs and the bare CNT webs performed in our previous study [21]. The electrochemical performance of CNT webs was described in our previous study [21], and the electrochemical performance of CuO materials was studied in the literature [35]. The CuO@CNT NCs gradually enhanced the capacity with an increase in the number of cycles, which showed a higher capacity than the bare CNT webs and the theoretical capacity of CuO. A capacity increase during the cycling has been reported with similar results with a porous carbon/tin composite [36], cubic and octahedral Cu_2O nanostructures [37], and carbon-coated CuO hollow spheres [38] in LIBs. The mechanism of the capacity increase was reported as a result of the reversible formation of gel-like polymeric species in SEI films induced by the catalytic activity of metals in the anodes [36,39]. We tried to interpret the capacity increase that was partially understood from the morphology change of the CuO anodes during the cycling, which we dealt with later in this study (in the section of "Microstructural changes of CuO@CNT NCs' electrodes").

Generally, the capacity decreases with an increase in the number of cycles. In addition, pulverization of an active material in an electrode during cycling is a critical issue that disrupts the electron path and rapidly decreases capacity [40-42]. However, it should be noted that the capacity showed a constant

increase from the 25th cycle in the CuO@CNT NCs electrode. Huang et al. [40] reported interesting results: The capacity increased after around 20 cycles, even though the electrodes experienced a structural change. They showed very similar results and trends we found in this study. It is interesting to note that the increment of the specific capacity in this study was much higher than Huang's result. Therefore, we assumed that there was an additional factor involved in the increased capacity. We discuss this assumption later. The discharge capacity in the first cycle was around 860 mAh g^{-1}, which was slightly higher than that of an electrode made by the slurry method using similar materials [17]. However, the coulombic efficiency (about 50%) was worse than that in Ko's study [17]. Thus, the CNT materials influenced the capacity as well as the coulombic efficiency. In our previous study, using pure CNT web resulted in a low coulombic efficiency due to the high surface area of the CNT webs electrode [21].

The different rate performance of the CuO@CNT NCs electrode at various current densities was explored as shown in Fig. 5d. First, the electrode was cycled at 0.5 C rate for 100 cycles before the rate capability test. Unlike the cycling performance cycled at the 0.5 C rate in Fig. 4c, the cycling performance at a 0.1 C rate exhibited a steady retention capacity with approximately 800 mAh g^{-1}. Even though a current collecting and/or conducting powder was absent during the electrode formation, the free-standing CuO@CNT NC electrode demonstrated an excellent high-rate of performance. After the current density returned to the 0.1 C rate, the capacity recovered to a higher level (around 1100 mAh g^{-1}) than the initial capacity at 0.1 C, which thus indicates that the CNT itself contributed to the capacity as an active electrode. In addition, the increase in the capacity suggests that the internal structure of this free-standing electrode changed and combined with CuO NPs.

To analyze the electrochemical performance of the free-standing electrode, electrochemical impedance spectroscopy was carried out with a free-standing CuO@CNT NCs electrode and a free-standing pure CNT web electrode (Fig. 6). Here, the high-frequency semicircle (in red) corresponds to the resistance R_f in the SEI layer, and the semicircle in the medium-frequency region (in blue) is assigned to the charge-transfer resistance R_{ct} at the electrode/electrolyte interface. The inclined line corresponds to the Li^+ diffusion process within the bulk of the electrode material.

As shown in Fig. 6a and b, the CuO@CNT NCs electrode revealed a much higher performance. The resistance at the SEI layer (R_f) and the charge-transfer resistance of the electrode/electrolyte interface (R_{ct}) in the CuO@CNT NCs electrode system showed a much lower value (R_f=12 vs. 33 and R_{ct} = 20 vs. 73), compared to the pure CNT web electrode. In addition, the inclined line of the CuO@CNT NCs electrode, which is attributed to the Li ion diffusion rate, appeared steeper than that of the pure CNT web electrode. As a result, this forest-like CuO@CNT NC is capable of accommodating Li ions with ease by demonstrating a free-standing electrode in terms of electric resistance and the diffusion of Li ions. According to the association of CuO NPs with a conducting CNT network structure, we can facilitate the features of both materials. In the role of an active material, the CuO in the CuO@CNT NCs electrode can lead to a higher capacity by taking advantage of the CuO capacity. On the other hand, the CNT webs confines the CuO NPs in their network structures and provides a good electron path.

3.3. Microstructural changes of CuO@CNT NC electrodes

Since the electrode did not undergo the slurry preparation steps (e.g., grinding, ball milling, mixing, etc.), it maintained the pristine structures of the CuO NRs (Fig. 7a). A high discharge capacity (863.7 mAh g^{-1}) was obtained from the first cycle; however, the cycling showed a significant irreversible capacity loss of around 50%. This irreversible capacity loss has been recognized by the formation of the SEI layer, which is easily created on the surface of an active carbon electrode [43]. The scanning electron microscope (SEM) images of the disassembled cell after 200 cycles showed the decomposed electrolyte of a gray-coated web (Fig. 7); here, SEI layers were observed on the surface of CuO@CNT NCs electrode (Fig. 7b). Many crater-shaped pores were created by the influence of an electron beam during the SEM characterization. The area of the smooth surface was enlarged to characterize the surface. There were many small CuO particles that were distributed throughout the area (Fig. 7c).

As shown in Fig. 8a, tiny CuO NPs were uniformly distrib-

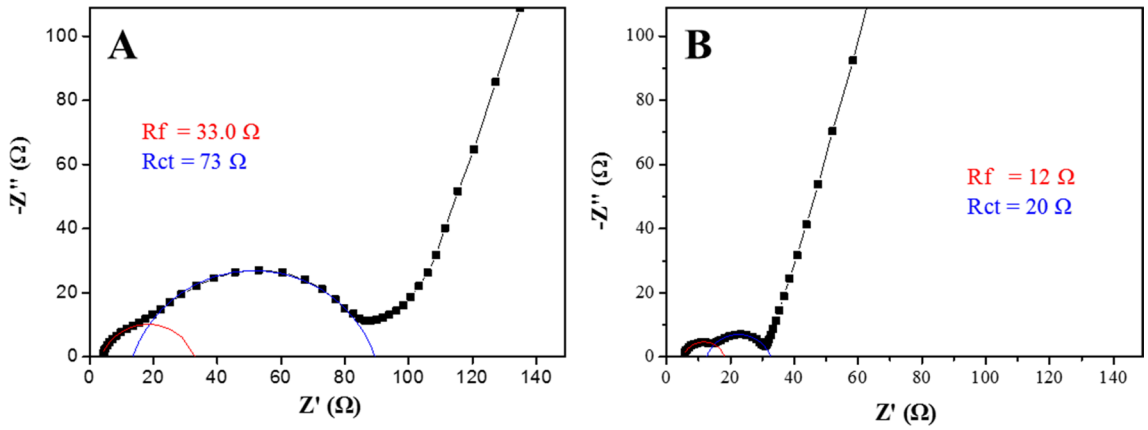

Fig. 6. Nyquist plots of a free-standing CNT web electrode (a) and a free-standing CuO@CNT NC electrode (b) after the 3rd cycle, by applying a sine wave with amplitude of 5.0 mV at a frequency range of 10 mHz to 0.1 MHz with a circuit model of this system.

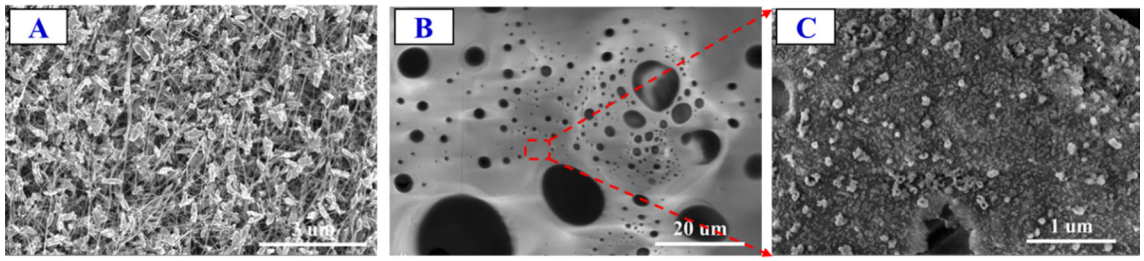

Fig. 7. SEM images of the forest-like CuO@CNT NCs (a) before cycling and (b, c) after 200 cycles.

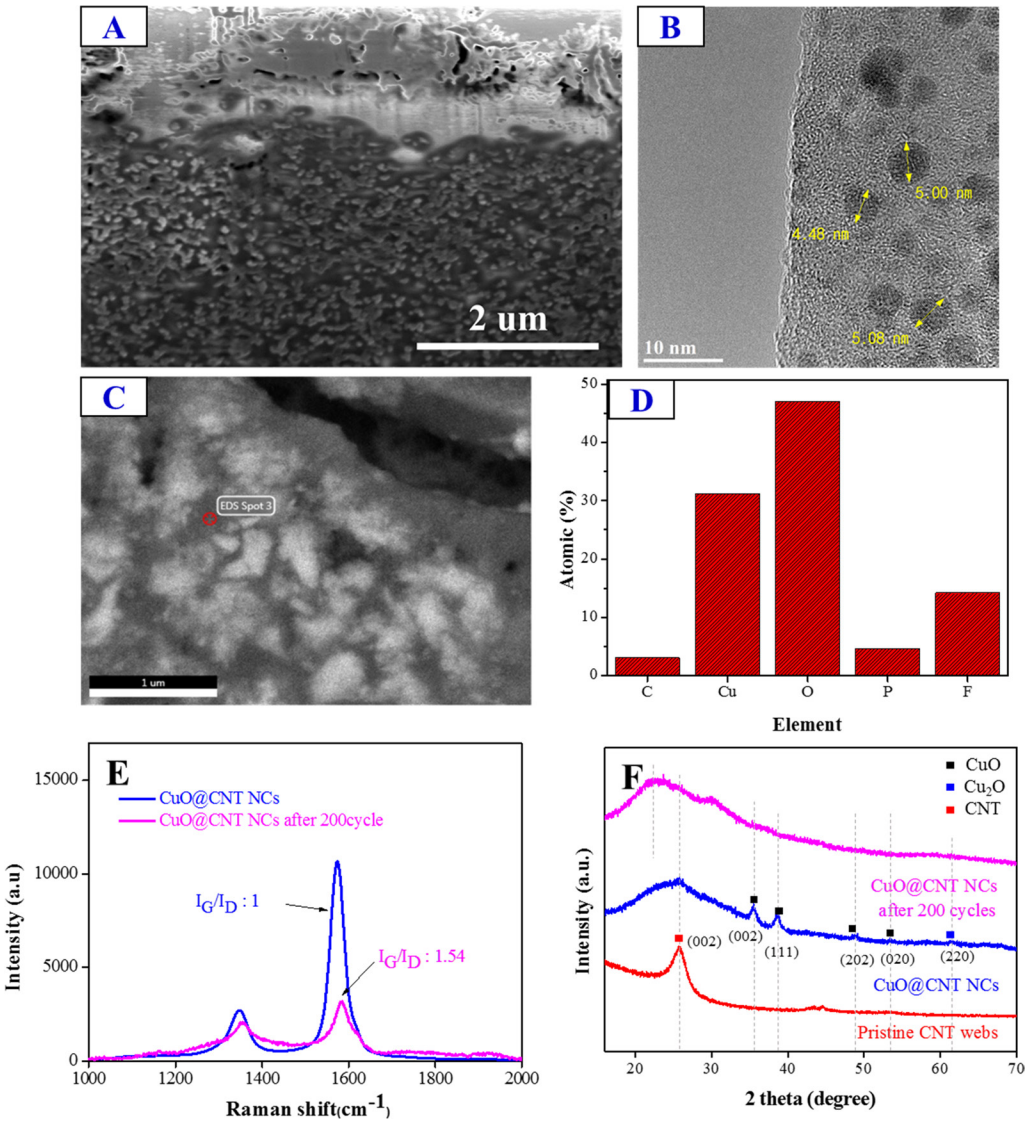

Fig. 8. Cross-section SEM image (a) of the CuO@CNT NC electrode after 200 cycles. TEM image (b) of a single CNT fiber from the CuO@CNT NC electrode after 200 cycles (B). SEM image (c) of the CuO@CNT NC electrode after 200 cycles for EDX evaluation and its result (d). Raman curves (e) and XRD profiles (f) to compare the internal structures of the pristine CuO@CNT NC electrode with those of the 200-cycled CuO@CNT NC electrode. The peak of the CNT@CNT NCs after 200 cycles at (002) shifted toward a low 2-theta angle.

uted throughout the cross-section of the CuO@CNT NC electrode. Thus, larger CuO particles were broken up into smaller CuO particles after 200 cycles. In the TEM image (Fig. 8b), there were small CuO particles on the surface of CNTs. Through the EDX, the gray area was verified to be filled with CuO materials. Due to the platinum coating as a protective layer during the

focused ion beam sample preparation, the platinum layer was formed on the top as shown in Fig. 8a.

At the 25th cycle, the increase of the specific capacity was due to an increment of active sites in the active materials. This can be inferred from the experimental data and is found in the literature [31,42,44,45]. For the experimental results, a higher portion of the CuO particles in the forest-like CuO@CNT NCs might have contributed to the cycling activities by disintegrating larger CuO NRs into tiny particles during cycling. Subsequently, these particles were imbedded into the CNT webs. This mechanism led to an increase of active sites in the CuO@CNT NC electrode, which eventually enhanced the accommodation of Li ions.

As the CuO NPs were embedded into the structures of the CNT webs, more CuO NPs became an active part of the electrode. The broken CuO particles were confirmed by SEM images of the CuO@CNT NC electrode in the disassembled cell after 200 cycles (Figs. 7c and 8a). The surface and cross section of the disassembled electrode showed that the tiny CuO NPs were distributed throughout; thus, there was a clear distinction between the images of the pristine CuO@CNT NC electrode. The three-dimensional network structure in the CNT webs was tightly packed with the broken CuO NPs, which created a good contact with the CNT material. Eventually, the electrons generated during the cycling were conveyed to the terminal of the LIBs. In addition, it is interesting to note that the CuO NPs (around 3–5 nm) imbedded in the CNT fibers maintained their size after many cycles (Figs. 3b and 8b). This indicates that the tiny size of the active materials allowed them to maintain their structure under the influence of volume expansion during the repeated cycling [40,46]. According to the XRD and Raman analyses of the CuO@CNT NC electrode after 200 cycles, the peak for carbon shifted into a lower 2-theta angle as shown in Fig. 8e and f. It might be inferred that the crystalline space was widened and the degree of crystalline perfection became lower from I_G/I_D ratio due to the intercalation of Li ions in the CNT fibers. In particular, the crystal peaks of the CuO@CNT NCs after 200 cycles disappeared, which indicated that the highly crystalline active copper oxide materials were decayed to amorphous structures during repeated cycles [40]. These experimental results confirmed that the reported data is in agreement with those described in a reference [40].

On the other hand, the nanostructured anodes, such as CuO and other metal oxide electrodes in LIBs, exhibited capacity fluctuation during cycling [31,46-48]. By consulting with other references [44,45], we can explain the capacity increase with two reasons. First, the electrochemically polymeric/gel-like layers were formed by electrolyte decomposition [44]; this formation is observed in our results of Fig. 7b. These layers enhanced the mechanical cohesion around the active anode, which gradually increased the capacity via "pseudo-capacitance-type behavior" [48,49]. Second, Z. Yang et al. [45] explained that the quasi-1-dimensional CuO NR anode provided a short lithium ion diffusion path and large specific surface area so that the lithiation reaction could take place more rapidly and efficiently. Z. Yang's explanation was confirmed by the SEM and TEM images of our experimental results, which showed numerous tiny CuO particles. This free-standing anode with a higher capacity is a promising candidate for a novel flexible LIB incorporated in a counterpart free-standing cathode.

4. Conclusions

We successfully designed and synthesized a forest-like CuO@CNT NC by developing CuO NRs on the surface of CNT fibers. The forest-like CuO@CNT NC was synthesized by taking advantage of CNT webs to create advantages such as a superb flexibility, high conductivity and an intermingled three-dimensional structure. This design of a free-standing CuO@CNT NC electrode showed its potential for use in flexible LIBs. In addition, the electrode illustrated a good rate capability and excellent cycling performance along with the comparable specific capacity; this was improved by an increase in the number of cycles due to the unique structure of CuO NRs in CNT webs. The proposed method is novel and very promising for a practical flexible/bendable full cell architecture with a combination of a free-standing anode and cathode.

Conflict of Interest

No potential conflict of interest relevant to this article was reported.

Acknowledgements

This work was supported by the Technology Innovation Industrial Program funded by the Ministry of Trade, Industry & Energy (MOTIE, Korea) (10052838, Development of the direct spinning process for continuous carbon nanotube fibers). This work was also partially supported by Korea Institute of Science and Technology Institutional program.

References

[1] Kwon YH, Woo SW, Jung HR, Yu HK, Kim K, Oh BH, Ahn S, Lee SY, Song SW, Cho J, Shin HC, Kim JY. Cable-type flexible lithium ion battery based on hollow multi-helix electrodes. Adv Mater, **24**, 5192 (2012). https://doi.org/10.1002/adma.201202196.

[2] Gwon H, Hong J, Kim H, Seo DH, Jeon S, Kang K. Recent progress on flexible lithium rechargeable batteries. Energy Environ Sci, **7**, 538 (2014). https://doi.org/10.1039/C3EE42927J.

[3] Noerochim L, Wang JZ, Chou SL, Wexler D, Liu HK. Free-standing single-walled carbon nanotube/SnO_2 anode paper for flexible lithium-ion batteries. Carbon, **50**, 1289 (2012). https://doi.org/10.1016/j.carbon.2011.10.049.

[4] Lee SW, Gallant BM, Lee Y, Yoshida N, Kim DY, Yamada Y, Noda S, Yamada A, Shao-Horn Y. Self-standing positive electrodes of oxidized few-walled carbon nanotubes for light-weight and high-power lithium batteries. Energy Environ Sci, **5**, 5437 (2012). https://doi.org/10.1039/C1EE02409D.

[5] Mukherjee M, Thomas AV, Krishnamurthy A, Koratkar N. Photothermally reduced graphene as high-power anodes for lithium-ion batteries. ACS Nano, **6**, 7867 (2012). https://doi.org/10.1021/nn303145j.

[6] Chen H, Müller MB, Gilmore KJ, Wallace GG, Li D. Mechanically strong, electrically conductive, and biocompatible graphene

paper. Adv Mater, **20**, 3557 (2008). https://doi.org/10.1002/adma.200800757.

[7] Novoselov KS, Geim AK, Morozov SV, Jiang D, Zhang Y, Dubonos SV, Grigorieva IV, Firsov AA. Electric field effect in atomically thin carbon films. Science, **306**, 666 (2004). https://doi.org/10.1126/science.1102896.

[8] Landi BJ, Ganter MJ, Schauerman CM, Cress CD, Raffaelle RP. Lithium ion capacity of single wall carbon nanotube paper electrodes. J Phys Chem C, **112**, 7509 (2008). https://doi.org/10.1021/jp710921k.

[9] Chew SY, Ng SH, Wang J, Novák P, Krumeich F, Chou SL, Chen J, Liu HK. Flexible free-standing carbon nanotube films for model lithium-ion batteries. Carbon, **47**, 2976 (2009). https://doi.org/10.1016/j.carbon.2009.06.045.

[10] Wang K, Luo S, Wu Y, He X, Zhao F, Wang J, Jiang K, Fan S. Super-aligned carbon nanotube films as current collectors for lightweight and flexible lithium ion batteries. Adv Funct Mater, **23**, 846 (2013). https://doi.org/10.1002/adfm.201202412.

[11] Wang C, Li D, Too CO, Wallace GG. Electrochemical properties of graphene paper electrodes used in lithium batteries. Chem Mater, **21**, 2604 (2009). https://doi.org/10.1021/cm900764n.

[12] Zhao Q, Gu ZN, Zhuang QK. Electrochemical study of tetra-phenyl-porphyrin on the SWNTs film modified glassy carbon electrode. Electrochem Commun, **6**, 83 (2004). https://doi.org/10.1016/j.elecom.2003.10.014.

[13] Geng HZ, Kim KK, So KP, Lee YS, Chang Y, Lee YH. Effect of acid treatment on carbon nanotube-based flexible transparent conducting films. J Am Chem Soc, **129**, 7758 (2007). https://doi.org/10.1021/ja0722224.

[14] Hellstrom SL, Lee HW, Bao Z. Polymer-assisted direct deposition of uniform carbon nanotube bundle networks for high performance transparent electrodes. ACS Nano, **3**, 1423 (2009). https://doi.org/10.1021/nn9002456.

[15] Jo JW, Jung JW, Lee JU, Jo WH. Fabrication of highly conductive and transparent thin films from single-walled carbon nanotubes using a new non-ionic surfactant via spin coating. ACS Nano, **4**, 5382 (2010). https://doi.org/10.1021/nn1009837.

[16] deHeer WA, Bacsa WS, Chatelain A, Gerfin T, Humphrey-Baker R, Forro L, Ugarte D. Aligned carbon nanotube films: production and optical and electronic properties. Science, **268**, 845 (1995). https://doi.org/10.1126/science.268.5212.845.

[17] Ko S, Lee JI, Yang HS, Park S, Jeong U. Mesoporous CuO particles threaded with CNTs for high-performance lithium-ion battery anodes. Adv Mater, **24**, 4451 (2012). https://doi.org/10.1002/adma.201201821.

[18] Morales J, Sánchez L, Martín F, Ramos-Barrado JR, Sánchez M. Nanostructured CuO thin film electrodes prepared by spray pyrolysis: a simple method for enhancing the electrochemical performance of CuO in lithium cells. Electrochim Acta, **49**, 4589 (2004). https://doi.org/10.1016/j.electacta.2004.05.012.

[19] Feng JK, Xia H, Lai MO, Lu L. Electrochemical performance of CuO nanocrystal film fabricated by room temperature sputtering. Mater Res Bull, **46**, 424 (2011). https://doi.org/10.1016/j.materresbull.2010.12.006.

[20] Chen HY, Mai JC. 22nd International Symposium on Plasma Chemistry, Belgium, (2015).

[21] Yoon S, Lee S, Kim S, Park KW, Cho D, Jeong Y. Carbon nanotube film anodes for flexible lithium ion batteries. J Power Sources, **279**, 495 (2015). https://doi.org/10.1016/j.jpowsour.2015.01.013.

[22] Jung Y, Song J, Huh W, Cho D, Jeong Y. Controlling the crystalline quality of carbon nanotubes with processing parameters from chemical vapor deposition synthesis. Chem Eng J, **228**, 1050 (2013). https://doi.org/10.1016/j.cej.2013.05.088.

[23] Song J, Yoon S, Kim S, Cho D, Jeong Y. Effects of surfactant on carbon nanotube assembly synthesized by direct spinning. Chem Eng Sci, **104**, 25 (2013). https://doi.org/10.1016/j.ces.2013.09.008.

[24] Luo YH, Huang J, Jin J, Peng X, Schmitt W, Ichinose I. Formation of positively charged copper hydroxide nanostrands and their structural characterization. Chem Mater, **18**, 1795 (2006). https://doi.org/10.1021/cm052270s.

[25] Song S, Kim S, Yoon S, Cho D, Jeong Y. Enhanced spinnability of carbon nanotube fibers by surfactant addition. Fibers Polym, **15**, 762 (2014). https://doi.org/10.1007/s12221-014-0762-2.

[26] Favors Z, Bay HH, Mutlu Z, Ahmed K, Ionescu R, Ye R, Ozkan M, Ozkan CS. Towards scalable binderless electrodes: carbon coated silicon nanofiber paper via Mg reduction of Electrospun SiO_2 Nanofibers. Sci Rep, **5**, 8246 (2015). https://doi.org/10.1038/srep08246.

[27] Kim SY, Yang KS, Kim BH. Improving the microstructure and electrochemical performance of carbon nanofibers containing graphene-wrapped silicon nanoparticles as a Li-ion battery anode. J Power Sources, **273**, 404 (2015). https://doi.org/10.1016/j.jpowsour.2014.09.109.

[28] Cheng HM, Li F, Su G, Pan HY, He LL, Sun X, Dresselhaus MS. Large-scale and low-cost synthesis of single-walled carbon nanotubes by the catalytic pyrolysis of hydrocarbons. Appl Phys Lett, **72**, 3282 (1998). https://doi.org/10.1063/1.121624.

[29] Saito R, Jorio A, Hafner JH, Lieber CM, Hunter M, McClure T, Dresselhaus G, Dresselhaus MS. Chirality-dependent G-band Raman intensity of carbon nanotubes. Phys Rev B, **64**, 085312 (2001). https://doi.org/10.1103/PhysRevB.64.085312.

[30] Wang C, Higgins D, Wang F, Li D, Liu R, Xia G, Li N, Li Q, Xu H, Wu G. Controlled synthesis of micro/nanostructured CuO anodes for lithium-ion batteries. Nano Energy, **9**, 334 (2014). https://doi.org/10.1016/j.nanoen.2014.08.009.

[31] Chen L, He H, Yu H, Cao Y, Lei D, Menggen Q, Wu C, Hu L. Electron field emission characteristics of graphene/carbon nanotubes hybrid field emitter. J Alloy Comp, **610**, 659 (2014). https://doi.org/10.1016/j.jallcom.2014.04.202.

[32] Bai Z, Zhang Y, Zhang Y, Guo C, Tang B. A large-scale, green route to synthesize of leaf-like mesoporous CuO as high-performance anode materials for lithium ion batteries. Electrochim Acta, **159**, 29 (2015). https://doi.org/10.1016/j.electacta.2015.01.188.

[33] Kim SJ, Lee AY, Park HC, Kim SY, Kim MC, Lee JM, Kim SB, Kim WS, Jeong Y, Park KW. Carbon nanotube web-based current collectors for high-performance lithium ion batteries. Mater Today Commun, **4**, 149 (2015). https://doi.org/10.1016/j.mtcomm.2015.06.010.

[34] Abbas SM, Hussain ST, Ali S, Abbas F, Ahmad N, Ali N, Khan Y. One-pot synthesis of a composite of monodispersed CuO nanospheres on carbon nanotubes as anode material for lithium-ion batteries. J Alloys Compd, **574**, 221 (2013). https://doi.org/10.1016/j.jallcom.2013.04.197.

[35] Seo SD, Jin YH, Lee SH, Shim HW, Kim DW. Low-temperature synthesis of CuO-interlaced nanodiscs for lithium ion battery electrodes. Nanoscale Res Lett, **6**, 397 (2011). https://doi.org/10.1186/1556-276X-6-397.

[36] Xu Y, Guo J, Wang C. Sponge-like porous carbon/tin composite

anode materials for lithium ion batteries. J Mater Chem, **22**, 9562 (2012). https://doi.org/10.1039/C2JM30448A.

[37] Kim MC, Kim SJ, Han SB, Kwak DH, Hwang ET, Kim DM, Lee GH, Choe HS, Park KW. Cubic and octahedral Cu_2O nanostructures as anodes for lithium-ion batteries. J Mater Chem A, **3**, 23003 (2015). https://doi.org/10.1039/C5TA05455A.

[38] Xu Y, Jian G, Zachariah MR, Wang C. Nano-structured carbon-coated CuO hollow spheres as stable and high rate anodes for lithium-ion batteries. J Mater Chem A, **1**, 15486 (2013). https://doi.org/10.1039/C3TA13698A.

[39] Su D, Xie X, Dou S, Wang G. CuO single crystal with exposed {001} facets: a highly efficient material for gas sensing and Li-ion battery applications. Sci Rep, **4**, 5753 (2014). https://doi.org/10.1038/srep05753.

[40] Huang ZX, Wang Y, Wong JI, Shi WH, Yang HY. Synthesis of self-assembled cobalt sulphide coated carbon nanotube and its superior electrochemical performance as anodes for Li-ion batteries. Electrochim Acta, **167**, 388 (2015). https://doi.org/10.1016/j.electacta.2015.03.183.

[41] Su Q, Xie J, Zhang J, Zhong Y, Du G, Xu B. In situ transmission electron microscopy observation of electrochemical behavior of CoS_2 in lithium-ion battery. ACS Appl Mater Interfaces, **6**, 3016 (2014). https://doi.org/10.1021/am4056084.

[42] Cabana J, Monconduit L, Larcher D, Palacín MR. Beyond intercalation-based Li-ion batteries: the state of the art and challenges of electrode materials reacting through conversion reactions. Adv Mater, **22**, E170 (2010). https://doi.org/10.1002/adma.201000717.

[43] Jeong SK. Mechanism of surface film formation on graphite negative electrodes and its correlation with electrolyte in lithium secondary batteries. J Korean Electrochem Soc, **13**, 19 (2010). https://doi.org/10.5229/JKES.2010.13.1.019.

[44] Yin Z, Ding Y, Zheng Q, Guan L. CuO/polypyrrole core–shell nanocomposites as anode materials for lithium-ion batteries. Electrochem Commun, **20**, 40 (2012). https://doi.org/10.1016/j.elecom.2012.04.005.

[45] Yang Z, Wang D, Li F, Liu D, Wang P, Li X, Yue H, Peng S, He D. Facile synthesis of CuO nanorod for lithium storage application. Mater Lett, **90**, 4 (2013). https://doi.org/10.1016/j.matlet.2012.09.006.

[46] Poizot P, Laruelle S, Grugeon S, Dupont L, Tarascon JM. Nano-sized transition-metal oxides as negative-electrode materials for lithium-ion batteries. Nature, **407**, 496 (2000). https://doi.org/10.1038/35035045.

[47] Shi Y, Guo B, Corr SA, Shi Q, Hu YS, Heier KR, Chen L, Seshadri R, Stucky GD. Ordered mesoporous metallic MoO_2 materials with highly reversible lithium storage capacity. Nano Lett, **9**, 4215 (2009). https://doi.org/10.1021/nl902423a.

[48] Wang Z, Luan D, Madhavi S, Hu Y, Lou XW. Assembling carbon-coated α-Fe_2O_3 hollow nanohorns on the CNT backbone for superior lithium storage capability. Energy Environ Sci, **5**, 5252 (2012). https://doi.org/10.1039/C1EE02831F.

[49] Débart A, Dupont L, Poizot P, Leriche JB, Tarascon JM. A Transmission electron microscopy study of the reactivity mechanism of tailor-made CuO particles toward lithium. J Electrochem Soc, **148**, A1266 (2001). https://doi.org/10.1149/1.1409971.